REGULAR ARTICLE

A reinvestigation of the deceptively simple reaction of toluene with OH, and the fate of the benzyl radical: a combined thermodynamic and kinetic study on the competition between OH-addition and H-abstraction reactions

Zoi Salta[1] · Agnie M. Kosmas[2] · Marc E. Segovia[3] · Martina Kieninger[3] · Oscar N. Ventura[3] · Vincenzo Barone[1]

Abstract

This work reports density functional and composite model chemistry calculations performed on the reactions of toluene with the hydroxyl radical. Both the experimentally observed H-abstraction from the methyl group and possible OH-additions to the phenyl ring were investigated. Reaction enthalpies and barrier heights suggest that H-abstraction is more favorable than OH-addition to the ring. The calculated reaction rates at room temperature and the radical-intermediate product fractions support this view. At first sight, this might seem to disagree with the fact that, under most experimental conditions, cresols are observed in a larger concentration than benzaldehyde. Since the accepted mechanism for benzaldehyde formation involves H-abstraction, a contradiction arises that calls for a more elaborate explanation. In this first exploratory study, we provide evidence that support the preference of H-abstraction over OH-addition and present an alternative mechanism which shows that cresols can be actually produced also through H-abstraction and not only from OH-addition, thus justifying the larger proportion of cresols than benzaldehyde among the products.

Keywords Toluene · Hydroxyl radical · Photodegradation · Atmospheric chemistry · Density functional methods

✉ Zoi Salta
   Zoi.Salta@sns.it

✉ Oscar N. Ventura
   Oscar.N.Ventura@gmail.com

✉ Vincenzo Barone
   Vincenzo.Barone@sns.it

1   SMART Lab, Scuola Normale Superiore, Piazza dei Cavalieri 7, 56126 Pisa, Italy

2   Physical Chemistry Sector, Department of Chemistry, University of Ioannina, 45110 Ioannina, Greece

3   Computational Chemistry and Biology Group, Facultad de Química, CCBG – DETEMA, UdelaR, CC1157, Montevideo 11000, Uruguay

1 Introduction

Atmospheric chemistry is a subject of paramount importance and increasing research interest since the '70 s of the last century [1–3]. Thousands of reactions, giving products and intermediate species of great relevance, both under daylight and nighttime conditions, have been the focus of extensive studies [3], ranging from anthropogenic climate change to aerosols, from ozone hole to pesticides, and from dioxines to volatile organic compounds in the atmosphere. Toluene is the simplest aromatic molecule with a side carbon chain, allowing competition between hydrogen abstraction and ring addition of OH. It is also one of the main anthropogenic aromatic molecules in the atmosphere, due to car exhaust, solvent use and biomass burning. Therefore, it has been studied repeatedly, both experimentally and theoretically [4–7]. A general consensus exists that addition of OH to the ring and H-abstraction from the methyl group are the main reaction channels, the former being apparently faster

than the latter. However, the detailed mechanism of toluene oxidation in the atmosphere remains uncertain [8, 9].

Davis et al. [10] were the first to determine the absolute rate constants for the reactions of the hydroxyl radical with benzene and toluene at 300 K. They obtained values of 1.59×10^{-12} and $(6.11 \pm 0.40) \times 10^{-12}$ cm^3 molecule^{-1} s^{-1}, respectively, with the latter result corresponding to global H-abstraction (rate constant k_{1a}) and ring addition reactions (rate constant k_{1b}) at a total pressure of 100 Torr of He. They interpreted these data in terms of hydroxyl radical reaction with toluene both through pressure-dependent OH-addition to the aromatic ring and via pressure-independent hydrogen abstraction from the side-chain methyl group. Other authors did similar experiments, simultaneously or shortly afterward, studying different aspects of the gas-phase reaction [11–13]. Tully et al. [14] investigated toluene and several deuterium substituted isomers to explore also the competition between OH-addition and H-abstraction. At low temperatures (250–298 K) they found an activation energy of 0.54 ± 0.44 kcal mol^{-1} and a rate constant of $(6.36 \pm 0.69) \times 10^{-12}$ cm^3 molecule^{-1} s^{-1}. With respect to the mechanism, they concluded that the addition reactions are predominant at low temperatures (below 298 K) while abstraction from the methyl group (and, in a small proportion, from the ring) prevails over 500 K.

Gery et al. [15] studied the gas-phase reaction of toluene and the hydroxyl radical generated in situ in a continuous stirred tank reactor by the photolysis of nitric acid. Leaving aside the reactions producing nitro-derivatives, the authors identified not only benzaldehyde but also cresols and small molecules like glyoxal and methylglyoxal, presumably arising from secondary reactions. They concluded that the H atom abstraction reaction, leading to benzaldehyde after further reaction with O$_2$, occurred with a 13 ± 4% total yield, while the addition reactions producing the cresols occurred with a 83 ± 4% total yield.

Hatipoglu et al. [16] performed a study of the photo-oxidative degradation of toluene in aqueous solution by the hydroxyl radical. In this combined experimental/theoretical study they used ultraviolet excitation of nitrate as a source of OH radicals to generate the products. Benzaldehyde and cresols were observed as final products, with yields of 30.5 ± 6.0% for o-cresol (the dominant pathway according to the DFT calculations presented), 47.0 ± 10.1% for the combined m- and p-cresols and 17.0 ± 3.3% for benzaldehyde.

Zhang et al. [17] studied experimentally the ring versus side-chain attack of substituted benzenes via dual stable isotope analysis. In the case of toluene, they concluded that there is a dominant role of aromatic ring OH-addition over abstraction, at variance with xylene isomers and anisole. A plot of $\Delta \delta^2 H$ vs. $\Delta \delta^{13} C$ showed that the behavior of toluene is similar to that of benzene and intermediate between the behaviors of nitrobenzene and ethylbenzene, with all these plots showing

a negative slope implying that addition is more favorable than abstraction.

A first quantum mechanical (MPn and B3LYP) study of the addition products was performed by Uc et al. [18]. While unlikely and not observed experimentally, they suggested the possibility that an *ipso* addition product would be collaborating to the experimentally observed high yield of o-cresol. Another theoretical study, this time on the fate of the benzyl radical under reaction with the oxygen molecule, was performed at the CBS-QB3 level by Murakami et al. [19]. Although thermochemical results were compatible with previous information, the data obtained for the possible dissociation channels, including benzaldehyde formation, were not conclusive. A slightly more sophisticated theoretical study of the oxidation of the benzyl radical was performed by da Silva et al. [20] using the G3B3 method. The novelty of this study was the inclusion of the benzyl hydroperoxide stable intermediate into the mechanism at high temperatures.

Very recently, the most comprehensive experimental/theoretical study of the atmospheric oxidation mechanism of toluene, performed by Ji et al. [21] arrived to different conclusions. They predicted that phenolic compounds rather than the peroxy radicals represent the dominant products and their experimental work suggested that there is a larger yield of cresols and a negligible formation of ring-cleavage products like methylglyoxal. The most recent theoretical study, performed by Zhang, Truhlar and Xu using DFT methods (M06-2X/MG3S and M08-SO/MG3S) [22], concluded that "abstraction of H from the methyl should not be neglected in atmospheric chemistry, even though the low-temperature results are dominated by addition".

To summarize the available information, one can say that there are three different situations in which the reaction of toluene with hydroxyl radicals could be significant: high temperature (combustion), gas phase (atmospheric) and aqueous solution. Leaving aside the high temperature situation, the experimental and theoretical information available until now gives slightly contradictory information concerning: (i) the appearance or not of ring-cleavage products, (ii) the paths leading to benzyl alcohol and benzaldehyde, (iii) the main pathways in the absence of NO$_x$ radicals and iv) the detailed mechanism of secondary reactions with hydroxyl radical and oxygen. It is the purpose of this paper to analyze in depth the existing evidence and to find all possible pathways for the oxidation of toluene in the absence of NO$_x$ radicals in gas phase, by investigating the competing OH-addition and H-abstraction reactions from both the thermodynamic and kinetic point of view.

2 Theoretical and computational details

It is well-known that the results obtained by state-of-the-art quantum mechanical methods, for instance CCSDTQ with a complete basis set (CBS), are very accurate (unless static correlation plays an overwhelming role). However, this approach is impractical for all except the smallest molecules. Thus, some kind of approximation has to be used. The simplest molecular orbital post Hartree–Fock model is based on second order Møller–Plesset perturbation theory (MP2) [23]. However, since this approach is normally not very accurate for radicals, the corresponding results are not reported in this study. Density functional (DFT) and quantum chemistry composite methods were used instead.

Equilibrium geometries, thermodynamic and kinetic properties were systematically obtained using DFT. We chose the M06 exchange–correlation functional [24], in view of its accurate description of main-group bond energies (Mean Unsigned Error = 1.8 kcal mol^{-1}) and non-covalent interactions (MUE = 0.4 kcal mol^{-1}). The M06 method depends on parameters which were optimized using different basis sets. Since this is a factor that may influence our own results, we tried a limited variation of the basis sets employed. We selected the 6-311++G(3df,2pd) [25] basis set as the standard option, but performed also calculations using a smaller one, 6-31 + G(d,p) and a more sophisticated one, the cc-pVQZ Dunning basis set [26], to judge the variability of our results with the basis set. Since during the preparation of this manuscript we became aware of a paper by Truhlar and coworkers showing the excellent performance of the M06-2X functional [22], we included also this DFT method in our study.

Furthermore, two composite models were used for the refinement of the energetic properties of the species involved, namely the CBS-QB3 method of Peterson et al. [27, 28] and the G4 method of Curtiss et al. [29]. These methods account for basis set extension and correlation energy effects by additive schemes on top of B3LYP equilibrium geometries and frequencies. Both of them are approximations, increasingly accurate, to CCSD(T)/CBS calculations, which are not feasible on molecules of this size. The estimated average errors of CBS-QB3 and G4 methods for a large series of molecules are below 2 kcal mol^{-1} and often around 1 kcal mol^{-1}.

Correlation energy within the composite methods mentioned above is obtained by different combinations of MP2, QCISD and CCSD(T) methods. In recent times, the powerful but costly CCSD(T)-f12 method [30], which includes the explicit non-averaged $1/r_{12}$ dependent correlation, has been successfully applied to many molecules. In this work we have applied the CCSD(T)-f12/cc-pVDZ-f12 method to some selected species, to further check our other calculations.

Most calculations have been carried out with the Gaussian 09 series of programs [31]. As usual, eigenvalues of the Hessian were checked for the critical points, to assure the correct number of negative eigenvalues for minima and transition states. Geometry optimizations were performed in all cases until Cartesian coordinates were accurate at least to 1×10^{-4} Å. An ultrafine grid was used for integration of the density in the density functional calculations. CCSD(T)-f12 single-point calculations at the M06-2X geometries were performed using the Molpro program [32] with the cc-pVDZ-f12 basis set, which is comparable to the jun-cc-pVTZ basis set employed in Ref. [22].

3 Results and discussion

The purpose of the study we are undertaking is to reanalyze the different reaction paths for the attack of toluene by the hydroxyl radical. Uc et al. [33] found that ring hydrogen abstraction is significant only at high temperatures. Therefore, we considered only H-abstraction from the methyl group and OH-additions to the ring. Secondary reactions with OH and O_2 were also included in the study. The set of reactions analyzed in our current publications on the subject is sketched in Scheme 1 below. No secondary reactions with NO_x radicals were considered up to now.

3.1 Thermodynamic point of view

The general reaction network presented in Scheme 1 is deceptively simple, but it actually masks a great deal of complexity. It can be decomposed, in principle, in two sets, one of ring-preserving reactions and another of ring breaking reactions. As products of the first reaction paths, one could obtain benzaldehyde, benzyl alcohol, cresols and other ring-preserving derivatives, as will be shown in a forthcoming publication. The second set of reactions would lead to glyoxal, methylglyoxal and other dialdehydes. Aromatic oxides are possible intermediates, even if later they would be easily transformed. The presence of OH, H_2O and O_2 in excess may lead to further reactions, eventually giving dihydroxylated products. Furthermore, the reaction of the benzyl radical with those species can lead to salicyl alcohol, benzoic acid, phenol, catechol, p-benzoquinone and bicyclic products. All reactants, products, intermediates and transition states for these reactions have been located and will be presented in a forthcoming publication.

The purpose of this publication is to study only the initial steps in the oxidation mechanism. However, it is necessary to discuss briefly how these reactions fit within the rest of the reaction paths, in order to appreciate the necessity of this
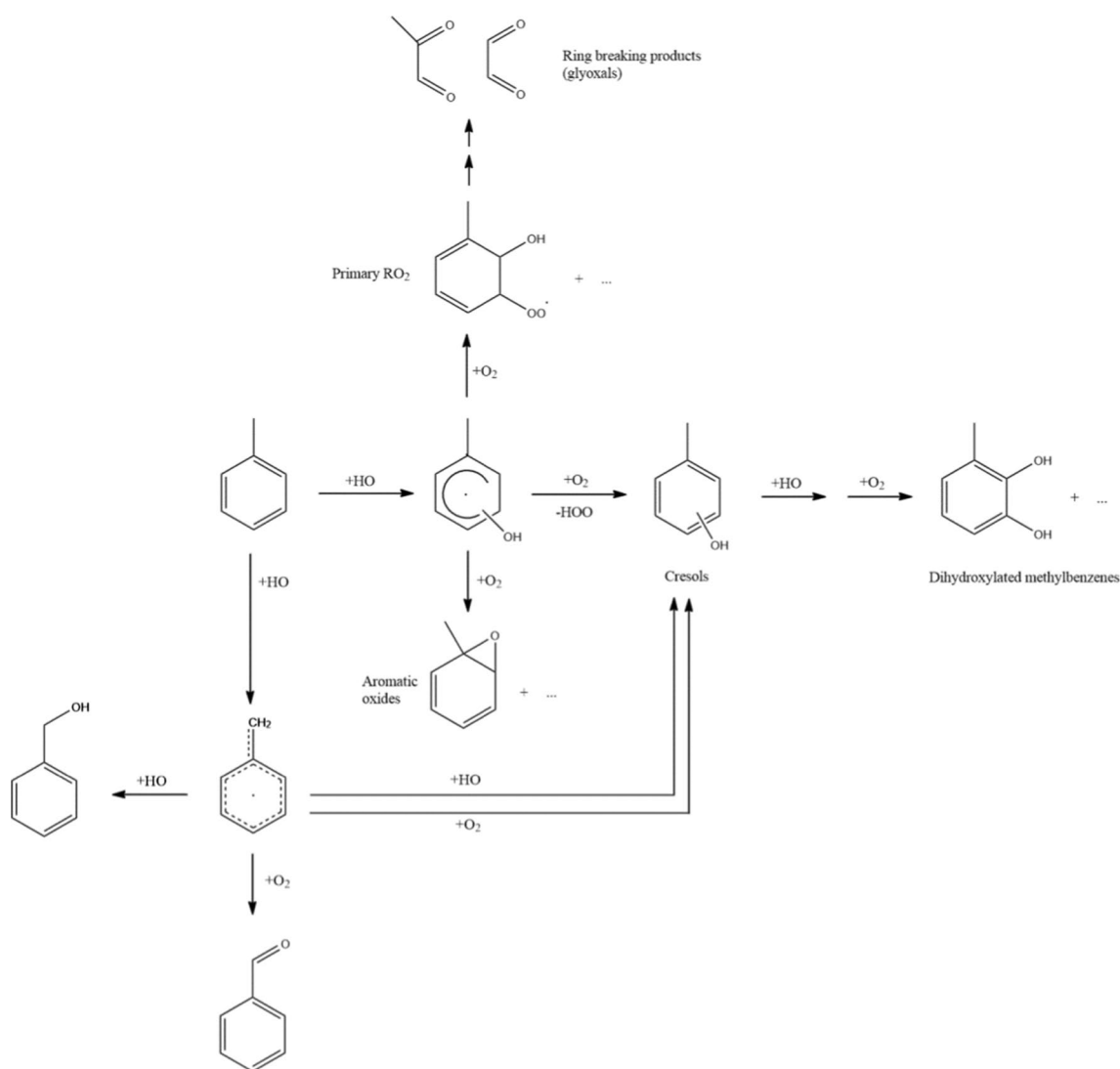
Scheme 1 Possible reaction paths after primary attack of the hydroxyl radical on toluene in the absence of NO$_x$ radicals

previous work. For that reason, we have included in the Supplementary Material section three schemes (Figures SM1–SM3) that summarize most of the reactions that are being studied at present. The mechanism is admittedly complex, and the nomenclature reflects this fact.

Figure SM2 shows the reaction paths leading essentially to cresols. Direct and indirect paths arising both from toluene (T) and the benzyl radical (TR) were uncovered. As was already known, hydroxyl addition to T produces the isomeric hydroxymethyl-cyclohexadienyl radicals (M03_oC, M18_pC, M37_mC) which may further react with oxygen (in the atmosphere) and/or with additional hydroxyl radicals, to produce diols (M16_oC, M25_pC, M44_mC) (in case of high concentration of hydroxyls or absence of oxygen in reaction chambers). Oxygen reactions may occur by direct H-abstraction (M06_oC, M21_pC, M36_mC) or by addition to the ring (M07_oC, M26_pC, M37_mC) and

further transformation. Addition at the *o-, m-* and *p-*positions may lead to cyclic peroxides by abstraction of an OH radical (M11_oC, M28_pC, M42_mC), while in the case of the addition at the *o-* or *p-* positions a secondary path was found. In these cases, internal transfer of a hydrogen atom and abstraction of an HOO˙ radical is a more energetically favorable path than direct H-abstraction by oxygen. This alternative path is not present in the route to obtain mC, and this might explain its lower concentration in the products.

Another thing we considered in this study is the possibility of reactions with a secondary hydroxyl radical that is regenerated during the process. The reaction of TR with excess hydroxyl radicals may lead to benzyl alcohol (M29_TR) by direct addition to the methylene moiety or, after addition to different positions at the ring (M12_oC, M22_pC, M44_mC), to the cresols themselves, by paths involving different bicyclic species. Two reaction paths

were found leading to *o*-cresol, two leading to *m*-cresol and only one leading to *p*-cresol. A full discussion of the energetics of the intermediates, products and transition states will be presented in a forthcoming publication.

On the other side, Fig. SM2 shows the reactions of TR with O_2 that we were able to identify theoretically. Benzyl radical can in principle react with the oxygen molecule at five different sites. It can be added at the methylene residue or at the *i*-, *o*-, *m*- and *p*-positions in the ring. The methylene carbon is the preferred site of addition by far. Therefore, the addition reaction paths to the ring were not investigated further in this paper. Reaction paths are labeled like in the paper by Hatipoglu et al. [16], when possible, to facilitate comparison, but several additional new routes and intermediates were identified. Contrary to what has been repeatedly described, the route leading to benzaldehyde is not the most favorable one (as we show in the explicit study of the mechanisms). A path involving conversion to benzoyl radical is preferred, probably with the intervention of catalytic water molecules. Other routes involving the appearance of catechol, salicyl alcohol, phenol, benzoquinone or other products are less probable. The importance of these reaction channels is that they lead to new products which may be experimentally identifiable under suitable conditions. The properties of some of the intermediates and products, like, e.g., their enthalpies of formation, were not until now established and had to be determined, either theoretically or experimentally. Our theoretical results on these species and the expected accuracy of the methodology employed in the whole work were analyzed and presented in an earlier publication [34].

Channel A in Fig. SM2 is of special interest, because only the breaking down of the benzyl peroxy radical to benzyloxy radical and oxygen was investigated previously. There is an obvious alternative route, which yields dibenzotetroxide by dimerization of the benzyl peroxy radical, and further reacts to give dibenzylperoxide and oxygen (see Fig. SM3). This mechanism, which may be important in the framework of combustion, has also been investigated in this study, but its discussion is postponed for an upcoming publication.

It is apparent from this discussion that the mechanism of reaction, in the presence of varying amounts of hydroxyl radicals and oxygen, is fairly complex. This complexity explains why different concentrations of products were obtained under different experimental conditions, in particular the proportion of cresols and benzaldehyde. Relative abundance of these products in a given experiment does not necessary correlate with the amount of TR and hydroxyl methylcyclohexadienyl radicals formed. Therefore, we focus only on the initial steps in these mechanisms in this communication, namely H-abstraction and OH-addition to toluene (see Scheme 2).

Pre-reactive complexes (PRCs) for this reactions presented a special challenge. In particular, only two PRCs were obtained for the interaction between T and OH using CBS-QB3, G4 or MP2 (*ortho* and *para*, see Fig. 1a–c) but less stable pre-reactive complexes at the *ipso* position and for the interaction with the CH_3 hydrogens at the opposite side of the ring were found at the M06 and M062X levels (see Fig. 1d–f).

The first complex shows a main interaction of OH with the *ortho* carbon atom (M01_oC, Fig. 1a), while the second does the same with the carbon at the *para* position (M17_pC, Fig. 1b). The spin distribution on these complexes shows that while M17_pC exhibits a well-localized OH fragment which will react mostly at the *para* position, M01_oC shows a much less bound OH, which has the ability to move nearer to the *ipso*, *ortho* or *meta* positions. The distance from the OH to the H atom in CH_3 is small enough to allow also the reaction of H-abstraction to occur (Fig. 1c).

Since the energies involved are small (see later on), the existence or not of these pre-reactive complexes might be masked by the inherent incertitude of the computational methods used. IRC calculations however show that at the M06/6-311++G(3df,2pd) level, a TS for abstraction of a methyl group hydrogen (TS01_TR) is obtained from the M01_oC PRC (see Fig. 2). Hatipoglu et al. [16] found pre-reactive complexes for each of the addition positions and the abstraction. However, their results are probably heavily influenced by the method used, B3LYP with the small 6-31G(d) basis set. In fact, comparing their p-PC complex with our equivalent M17_pC, one sees that they obtain an exceedingly short C-O distance, 1.918Å compared to our values of 2.393, 2.378, 2.356, 2.384, 2.428 and 2.698 Å, at the CBS-QB3, G4, M06 (with the three basis sets) and M062X/aug-cc-pVTZ methods, respectively. Uc et al. [33] used BHYandHLYP/6-311++G** method to obtain a Cs-symmetry structure for the abstraction, while Zhang et al. [22] determined that this structure is a TS at the M06-2X/MG3S level. Interestingly, Zhang et al. [22] did not find any other PRC and they assert that all reaction channels share the same pre-reactive complex. The authors made a comparison of the PRC they found with that of Uc et al. [33] in their Fig. 1; the distance between the oxygen atom and the hydrogen of the methyl group they found at the M06-2X/MG3S level is 2.953 Å, much smaller than that of Uc et al. and intermediate between the values we obtained at the M06/cc-pVQZ (2.827 Å) and M06-2X/aug-cc-pVTZ (3.046 Å) levels. Once again, this fact confirms that the general structure of the PRCs is heavily dependent on the method of calculation.

In addition to the previously described complexes, both M06 and M06-2X computations afforded another PRC structure, M01_TR, where the OH is weakly bound to the hydrogens of the methyl group. The OH moiety is
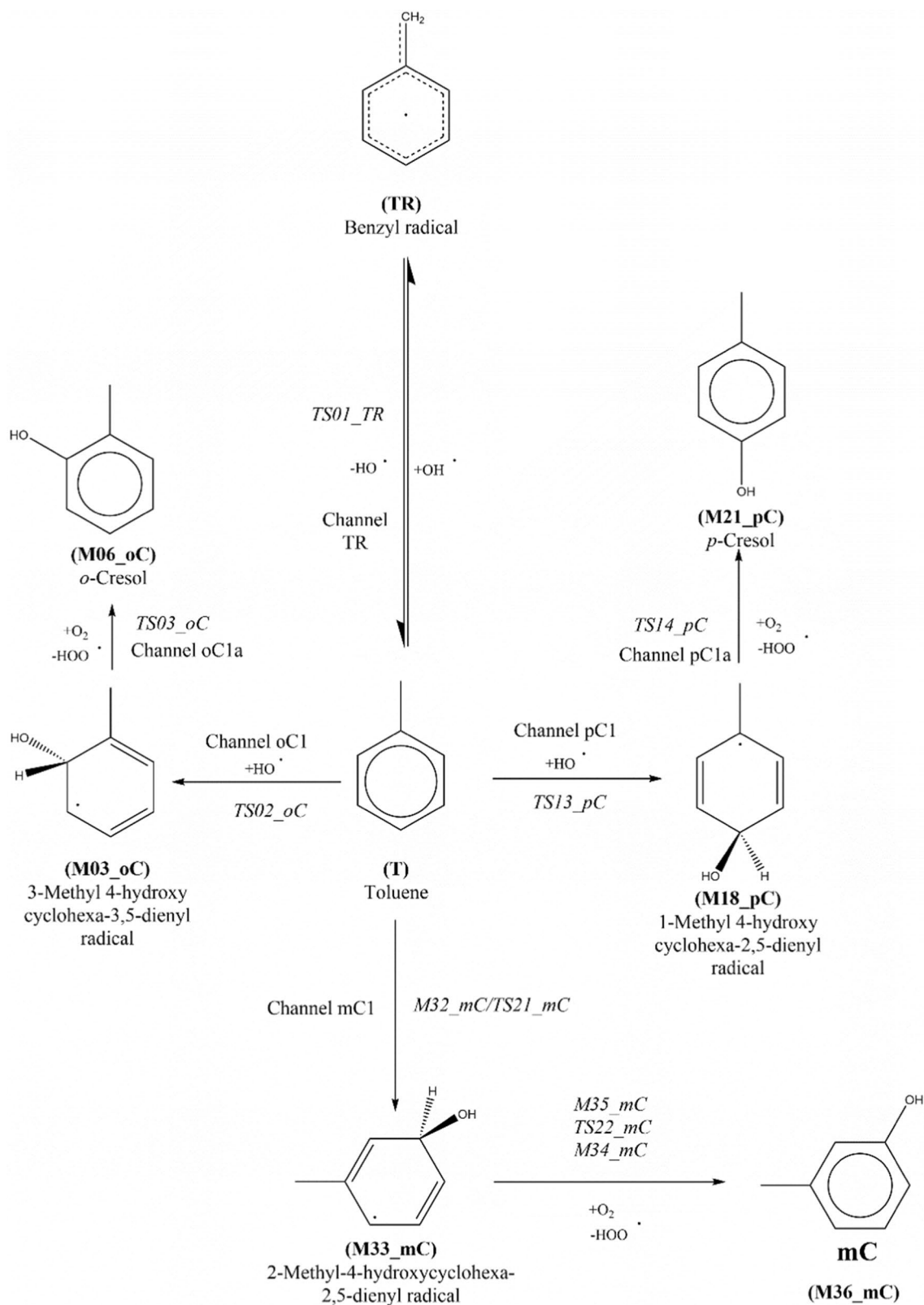
**Scheme 2** Initial steps in the OH-oxidation mechanism of toluene

Fig. 1 Structure of the pre-reactive complexes found. For both M01_oC (**1a**) and M17_pC (**1b**), a perspective view, a view from above the ring and the spin distribution are shown in the upper panel, while the most important parameters of both species are shown in the lower panel (**1c**), from top to bottom, each entry corresponds to G4, M06/6-311++G(3df,2pd), M06/cc-pVQZ and M06-2X/aug-cc-pVTZ optimized structures. The M06 and M06-2X structures of M01_TR are shown in (**1d**) and (**1e**) while side and top views of the M06_2X structure of the ipso complex is shown in (**1f**)
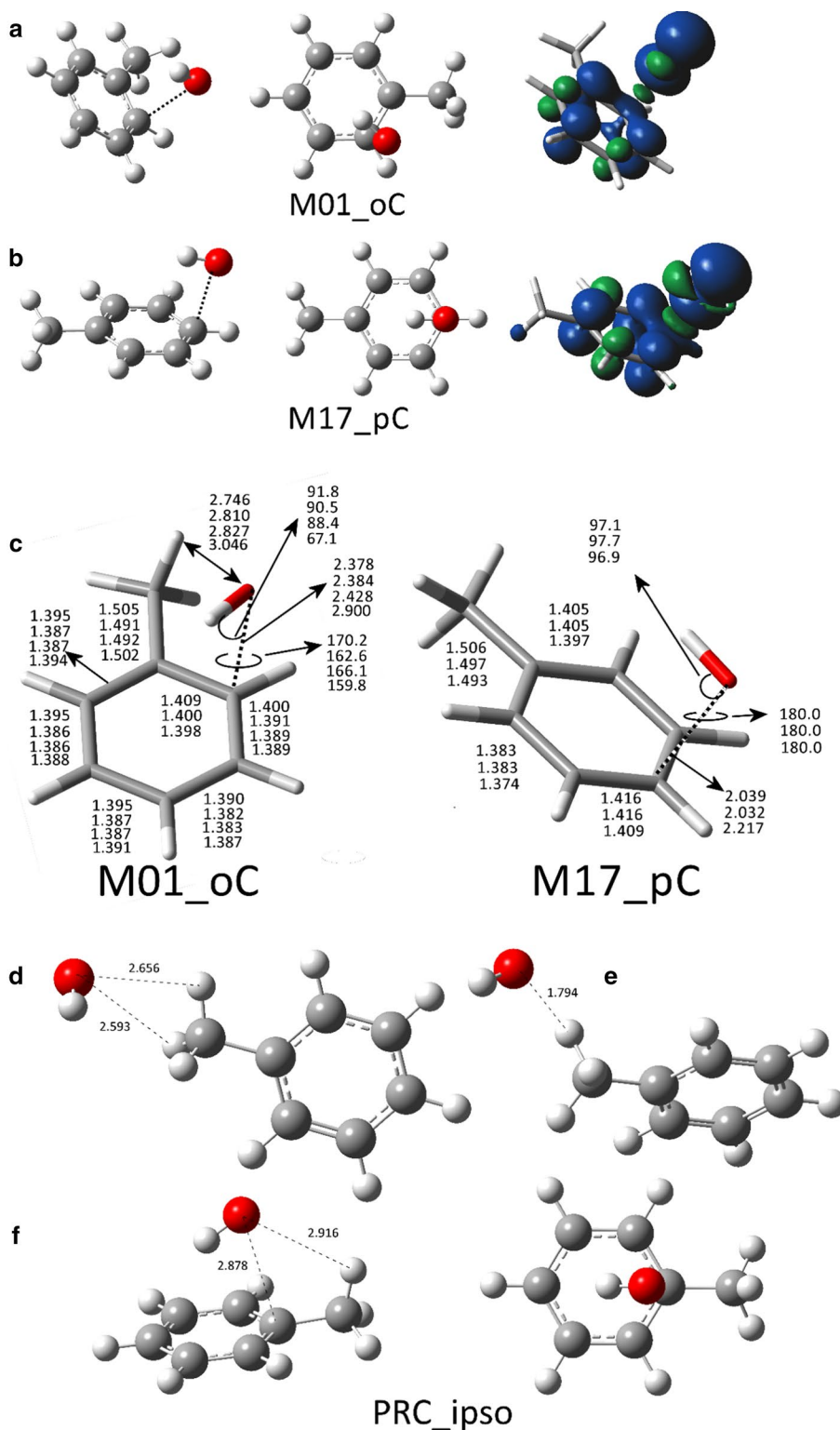
positioned at the opposite side of the ring along the C-CH$_3$ axis, thus avoiding any interaction that would lead to the addition isomers. This complex is weaker than the addition ones (see later on) and it is affected by the method used. While neither CBS or G4 reproduce it (because the geometry optimization within those composite methods is done at the B3LYP level), M06 affords a complex with only one clear O$\cdots$H interaction, while the M06-2X optimum structure presents two such interactions (see Fig. 1c,

Fig. 2 M06/cc-pVQZ IRC for the conversion of M01_TR to M02_TR, showing the very small height of the barrier
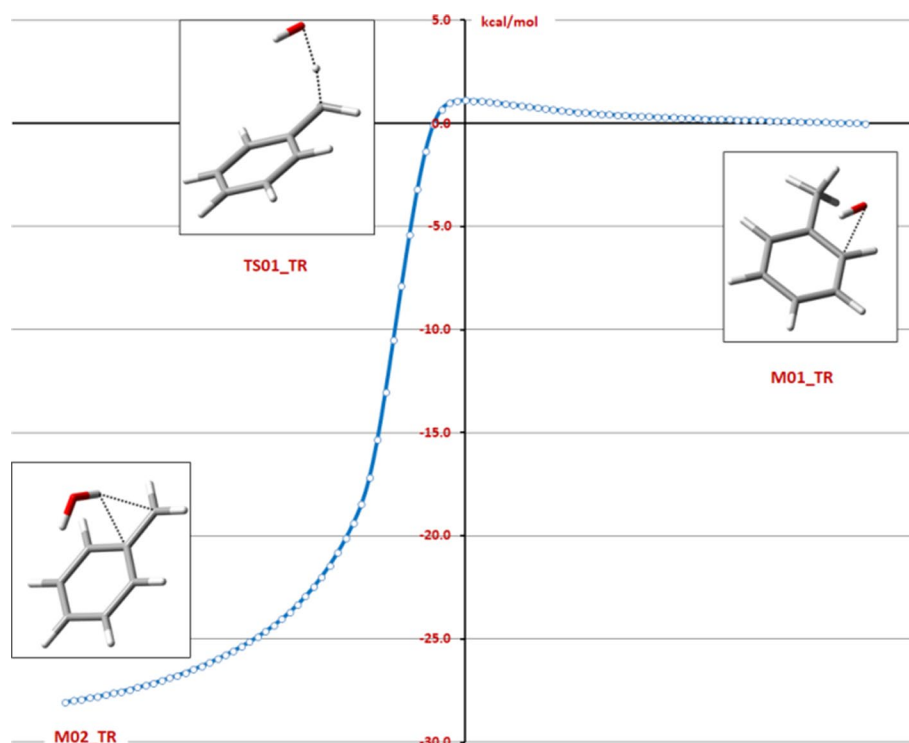
d). It is clear then again that an accurate structure cannot be precisely determined with the methods used.

Something similar occurs with the *ipso* complex, M01_iC (see Fig. 1e). It was located using the M06-2X method, but reverted back to M01_oC when either M06, CBS-QB3 or G4 were applied to the M06-2X optimum structure. Thus, in general, one can say that the theoretical methods used are not able to describe precisely the structure of the PRCs, a fact that has two consequences. On the one side, it does affect the shape of the PES and the precise structure of the initial complex. On the other side, since what is normally used for calculating reaction coefficients is the ZPE-corrected energy, the precise value is heavily dependent on a series of influences. A painstakingly detailed analysis, like the one done by Zhang and Truhlar [22] is necessary to approximate accurately the reaction properties.

In addition to the difficulties of the theoretical methods to locate precisely the structure of the pre-reactive complexes, the small interaction energies (see Table 1) imply that these PRCs would be of some interest only in gas phase at low temperatures. Gibbs energies at normal pressure and temperature are higher than those of the separated reactants, showing that the complexes are of marginal relevance for the reactions at room temperature (although they may be important in some regions of the atmosphere).

While OH-addition to the phenyl ring produces covalently bound product radicals (identified in the following as M03_oC, M18_pC and M33_mC for *o*-, *m*- and *p*-addition, respectively, see Scheme 2), H-abstraction obviously produces a vdW post-reactive complex (M02_TR) where a water molecule is non-covalently bound to the phenyl ring in the benzyl radical (TR). All four species are separated from the pre-reactive complexes by transition states (TS01_TR, TS02_oC, TS13_pC and TS21_mC see Scheme 2, Fig. 3 and Table 1). In the case of M02_TR, the final complex may be obtained either from M01_oC or M01_TR through two different transition states. However, the actual calculations show that the transition state coming from M01_oC is almost exactly the same as that coming from M01_TR. Interestingly, CBS-QB3 and G4 geometry optimizations of this TS also converge to a similar structure than those of the DFT methods, although M01_TR does not seem to be a minimum at these levels (both calculations end up giving the final complex M02_TR). Whether this situation is an artifact of the methods of calculation or a real feature of the potential energy surface we cannot say at the moment. In case it is a real feature, it has then implications for the whole kinetics of the process.

It is clear that the *ortho*, *meta* and *para* transition states have a similar structure, with the H atom of the hydroxyl radical pointing toward the π electronic cloud of the benzene ring, the oxygen placed directly on top of the C atom to which it will be added and with a COH angle of 90 deg. Once added, the OH group rotates and the OH bond points away from the cycle. Abstraction TS01_TR does also exhibit a general disposition of the OH bond toward the ring, while the H atom being transferred is midway between the C and O atoms.

Table 1 Energies (with respect to T + OH) of the pre-reactive complexes, transition states and products

Reaction	Species	Chemical model	ΔE_T	$\Delta(E_T+ZPE)$	$\Delta H(298)$	$\Delta G(298)$	E_a^a	$\Delta^{\ddagger}G^o(298)^b$
H-abstraction	M01_TR	CBS-QB3	nf					
		G4	nf					
		M06/6-311++G(3df,2pd)	−1.9	−1.2	−1.2	5.1		
		M06-2X/aug-cc-pVTZ	−1.6	−0.9	−0.6	4.8		
		CCSD(T)-f12/cc-pVDZ-f12	−1.1	−0.7	−0.3	5.1		
	TS01_TR[c]	CBS-QB3	1.2	1.3	1.1	7.9	2.8	7.9
		G4	−0.8	−0.5	−0.6	5.9	1.2	5.9
		M06/6-311++G(3df,2pd)	−2.0	−2.7	−3.5	4.9	2.7	4.9
							−1.5[d]	−0.2[d]
		M06/cc-pVQZ	−0.7	−1.9	−2.6	6.1	2.7	6.1
		M06-2X/aug-cc-pVTZ	1.1	0.3	−0.5	9.1	4.7	5.2
							1.2[d]	4.3[d]
		CCSD(T)-f12/cc-pVDZ-f12	1.2	0.5	0.3	8.7	4.3	5.0
							1.2[d]	3.6[d]
		CCSD(T)-F12a[e]		−0.5				
	M02_TR	CBS-QB3	−29.9	−28.8	−28.0	−23.1		
		G4	−30.9	−29.7	−29.0	−23.9		
		M06/6-311++G(3df,2pd)	−34.0	−33.1	−32.8	−27.6		
		M06/cc-pVQZ	−32.3	−31.4	−31.2	−24.3		
	TR + H$_2$O	CBS-QB3	−28.3	−28.5	−28.0	−29.4		
		G4	−28.1	−28.2	−27.7	−29.1		
		M06/6-311++G(3df,2pd)	−30.6	−30.7	−30.7	−30.5		
		M06/cc-pVQZ	−28.9	−29.0	−29.1	−28.1		
		M06-2X/aug-cc-pVTZ	−27.3	−27.7	−27.7	−26.5		
		CCSD(T)-f12/cc-pVDZ-f12	−28.5	−28.8	−28.9	−27.6		
		CCSD(T)-F12a[e]		−28.2				
o-Addition	M01_oC	CBS-QB3	−3.1	−1.5	−1.2	5.4		
		G4	−3.3	−1.7	−1.4	5.2		
		M06/6-311++G(3df,2pd)	−7.1	−5.5	−5.8	2.6		
		M06/cc-pVQZ	−6.1	−4.6	−4.8	3.9		
		M06-2X/aug-cc-pVTZ	−5.7	−4.4	−4.5	4.1		
		CCSD(T)-f12/cc-pVDZ-f12	−1.7	0.1	−0.7	8.1		
		CCSD(T)-F12a[e]		−4.8				
	TS02_oC	CBS-QB3	−3.0	−1.1	−1.5	7.0	0.4	7.0
		G4	−2.2	−0.4	−0.7	7.6	1.3	7.6
		M06/6-311++G(3df,2pd)	−6.2	−4.5	−5.4	4.7	1.0	4.7
		M06/cc-pVQZ	−4.9	−3.2	−4.2	6.6	1.4	6.6
		M06-2X/aug-cc-pVTZ	−3.5	−2.9	−3.1	5.5	2.2	5.5
		CCSD(T)-f12/cc-pVDZ-f12	−3.8	−3.1	−3.7	5.3	2.0	5.3
		CCSD(T)-F12a[e]		−1.7				
	M03_oC	CBS-QB3	−20.9	−18.0	−18.4	−9.8		
		G4	−20.6	−17.6	−18.1	−9.5		
		M06/6-311++G(3df,2pd)	−23.5	−20.5	−21.5	−11.3		
		M06/cc-pVQZ	−22.2	−19.3	−20.3	−9.3		
		CCSD(T)-F12a[e]		−21.7				
p-Addition	M17_pC	CBS-QB3	−2.3	−1.0	−1.1	5.8		
		G4	−3.4	−2.1	−2.1	4.5		
		M06/6-311++G(3df,2pd)	−5.9	−4.5	−4.6	2.7		
		M06/cc-pVQZ	−4.9	−3.8	−4.4	4.5		
	TS13_pC	CBS-QB3	−1.8	−0.2	−0.4	7.0	0.9	7.0

Table 1 (continued)

Reaction	Species	Chemical model	ΔE_T	$\Delta(E_T+ZPE)$	$\Delta H(298)$	$\Delta G(298)$	E_a^a	$\Delta^{\ddagger}G^o(298)^b$
		G4	−0.7	0.9	0.7	7.9	2.9	7.9
		M06/6-311++G(3df,2pd)	−4.7	−3.2	−3.9	5.2	1.3	5.2
		M06/cc-pVQZ	−3.4	−1.9	−3.3	8.2	1.9	8.2
		CCSD(T)-F12a[e]		−0.2				
	M18_pC	CBS-QB3	−19.7	−16.9	−17.2	−9.5		
		G4	−19.2	−16.5	−16.8	−9.4		
		M06/6-311++G(3df,2pd)	−22.1	−19.3	−20.1	−10.7		
		M06/cc-pVQZ	−20.7	−18.0	−18.8	−8.9		
		CCSD(T)-F12a[e]		−20.6				
m-Addition	TS21_mC	CBS-QB3	−1.5	0.2	−0.1	7.5	1.2	7.5
		G4	−0.4	1.2	1.0	8.5	3.3	8.5
		M06/6-311++G(3df,2pd)	−4.1	−2.4	−3.3	6.3	2.0	6.3
		M06/cc-pVQZ	−2.8	−1.2	−2.1	8.2	2.6	8.2
	M33_mC	CBS-QB3	−19.4	−16.6	−17.0	−8.5		
		G4	−19.1	−16.3	−16.7	−8.2		
		M06/6-311++G(3df,2pd)	−21.5	−18.6	−19.6	−9.5		
		M06/cc-pVQZ	−20.1	−17.4	−18.3	−7.5		
		CCSD(T)-F12a[e]		−20.4				

Activation energies and standard Gibbs energies of activation are also given. All values in kcal mol^{-1}

[a] $E_a = \Delta^{\ddagger}(E+ZPE)$ with respect to the pre-reactive complexes

[b] $\Delta^{\ddagger}G^o$ (298.15) with respect to T+OH

[c] Barriers for all entries are reported with respect to M01_oC

[d] for those methods for which the PRC M01_TR was found, a second line is included reporting the barrier with respect to this PRC

[e] jun-cc-pVTZ basis set from Ref. [22]

Fig. 3 Structure of the transition states and products formed in the H-abstraction from the methyl group and in the addition of OH to the ring at *ortho*, *meta* and *para* positions. Some important parameters are shown; the entries correspond to G4, M06/6-311++G(3df,2pd) and M06/cc-pVQZ calculations (from top to bottom)
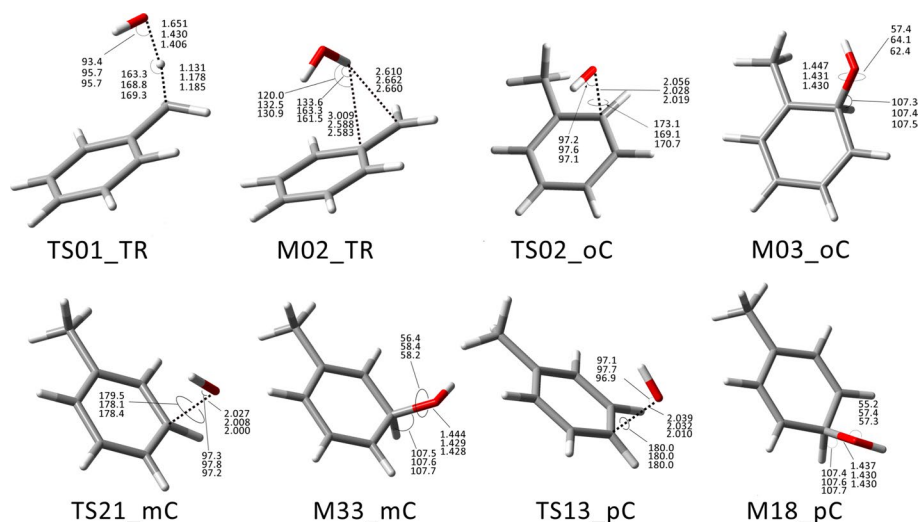
In the final complex, the water molecule lies in a plane nearly perpendicular to that of the TR plane, with one of the H atoms interacting with the cycle and the other with the methylene group. Some of the most interesting geometric features of the transition states and the final products for the three additions and the H-abstraction are shown in Fig. 3.

The optimized parameters support our previous assertions. In the case of the transition states, they are all between 160 and 180 degrees. In the case of TS01_TR and TS13_pC, the structures have a plane of symmetry containing the OH radical and bisecting the ring, while in the other two transition states, the OH is slightly tilted so that the H of OH points away from the methyl group. Once the addition

product has been formed, the local interaction between OH and the H on the same carbon forces the asymmetry of the group, with an angle that is between 55 and 62 degrees for all structures and methods. M02_TR is special of course, because the resulting product is a weakly bound complex (less than 2 kcal mol^{-1}, see Table 1) of the TR radical and water.

The data collected in Table 1 show that the different methods used in this work give a consistent picture of all the products. Formation of the benzyl radical, whether bound to the water molecule or not, is thermodynamically more favorable than the production of any of the addition radical adducts. This is a remarkable difference from the results reported by Hatipoglu et al. [16] which show an endothermic abstraction. The stability order of the addition products is, as expected from qualitative arguments, *ortho* < *para* < *meta*, all above the energy of the benzyl radical.

Moreover, it must be stressed that the results obtained at our best computational levels (G4 and M06/cc-pVQZ) are very close. Looking at the final radicals, for instance, the Gibbs energies of reaction are − 24.3, − 9.3, − 8.9, and − 7.5 kcal mol^{-1} at the M06/cc-pVQZ level for the abstraction, *o*-, *p*- and *m*-addition, respectively, while they are − 23.9, − 9.5, − 9.4 and − 8.2 kcal mol^{-1} at the G4 level. In all cases, the difference is below 1 kcal mol^{-1}. The differences are larger in the case of the initial complexes, a problem which is compounded by the already small value of the stabilization energies. This is also noticeable in the barriers, which end up showing in the activation energies, where discrepancies of up to 1.7 kcal mol^{-1} are observed. The differences are nonetheless smaller in the Gibbs energies of activation.

The picture of the interaction emerging from these results is that the OH radical tends to interact more strongly with the cycle than with the side methyl group. In this last case indeed, only some methods can locate the PRC, which is nonetheless about half as stable as the complexes of OH with the ring. The latter, in turn, all exhibit a marked interaction of the hydrogen atom in OH with the electron cloud above the cycle, the OH somehow pivoting on this H while the oxygen interacts with each possible carbon, giving origin to *ipso*, *ortho*, *meta* and *para* complexes. All these complexes are stable only at low temperatures, not at all at 298 K.

Perhaps the most striking result is that the transition state for the abstraction, TS01_TR, can be reached both from the PRC on the CH$_3$ side, M01_TR, and the *ortho* complex M01_oC. This is most probably a result of lack of sufficient discrimination by the theoretical methods used. In the following, we have chosen to compute the barriers with respect to M01_oC since nevertheless, this will be the most stable complex.

According to the previous discussion, from a purely thermodynamic point of view, the benzyl radical should be the

most abundant product, strongly prevailing over addition radicals. On the other side, the theoretical analogous to the experimental activation energy (i.e., $\Delta(E + \text{ZPE})$) is very similar at the best theoretical levels both for abstraction and *ortho* addition. These results deserve a more careful analysis from the point of view of kinetics.

3.2 Kinetic point of view

From the kinetic point of view, the situation is more complicated. First, one should notice that the activation energies are quite small, no matter which method is used for the calculation, and variations of up to 1.5 kcal mol^{-1} or slightly larger, are observed between methods for each of the isomeric transition states. This means that the ordering of the activation energies does depend heavily on the method and it even changes if one considers Gibbs energies of activation in place of activation energies. Considering the latter quantity, all methods but G4 agree that the smallest activation energy is that leading to the *ortho* addition. G4 predicts the abstraction to be favored instead. In the second place would be either *ortho* addition (G4) or *para* addition (all the other methods). Taking into account the Gibbs energies of activation instead, (which we will later use in the Eyring equation to obtain classical rate constants) we see that the G4 and M06/cc-pVQZ models agree in that the order of the barriers would be, from smaller to larger, H-abstraction, *o*-, *p*- and *m*-additions. It is also remarkable how the Gibbs energy of activation of the *ortho* addition increases within the M06 method when the basis set is augmented from 6-31 + G(d,p) to cc-pVQZ. In Fig. 4 are shown the $\Delta(E + \text{ZPE})$ and ΔG (298.15) profiles for the reactions, at the G4 and M06/cc-pVQZ levels for comparison purposes. It is clearly obvious that, even if at the $\Delta(E + \text{ZPE})$ profiles there are differences between the methods, the ΔG profiles are very similar and H-abstraction is clearly more favorable both thermodynamically and kinetically.

As a general conclusion, we can say that it is relatively easy to assess the stability of the four possible resulting radicals, but that it is very difficult to determine the barriers for the transformations, mainly because of the difficulty to calculate the stabilization energy of the PRCs. Perhaps, CCSD(T)/CBS calculations including core correlation, or beyond, can give a more precise estimation of the barriers but such calculations for these molecules are outside our present computational capabilities.

The fact that theoretical methods are not accurate enough for calculating the barriers has an effect in the calculation of the rate constants and the product fractions. Moreover, the combination of reasonably stable pre-reactive complexes at room temperature with low barriers, leads to negative activation energies for the reaction T + OH ⇄ PRC → TSs. Assuming that the reactants and PRC are in equilibrium,
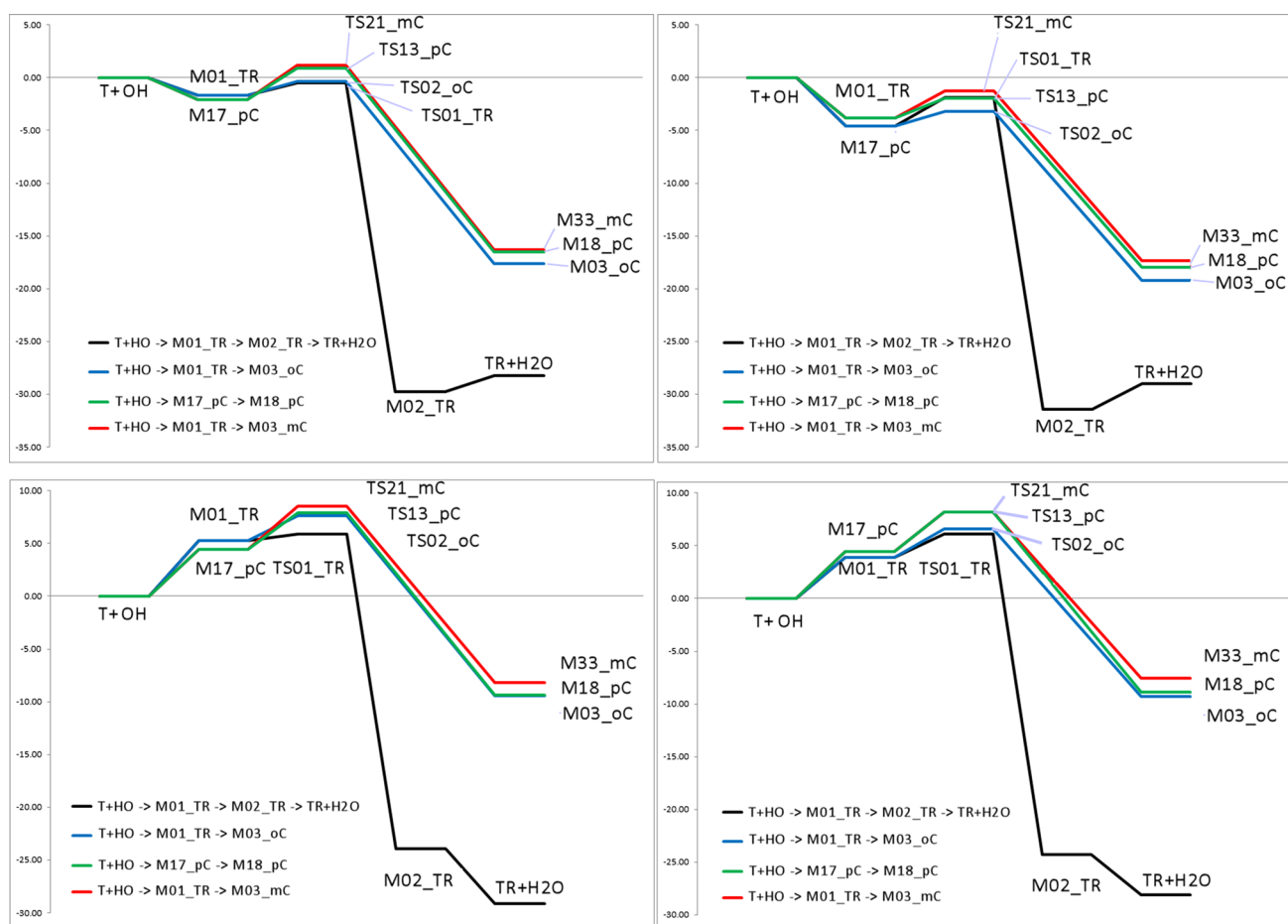
Fig. 4 Reaction profiles for the formation of the TR and o-, p- and m-hydroxymethylcyclodienyl radicals. Upper panels show energies $\Delta(E+\mathrm{ZPE})$, lower panels show Gibbs energies ΔG; G4 is at the left, M06/cc-pVQZ at the right

one can obtain the classical TST rate constant in the form of an Arrhenius equation:

$$k = \kappa \frac{k_B T}{h} \frac{Q_{TS}}{Q_T Q_{OH}} \exp\left(\frac{E_T + E_{OH} - E_{TS}}{RT} \right) \quad (1)$$

where the symbols have the usual meaning, κ is a tunneling factor, k_B, R and h are Boltzmann, gas, and Planck constants, respectively, T is the temperature, and Q_a and E_a are the partition function and energy of species a. The equation arises naturally from considering that k_{-1} (the reverse rate constant for the equilibrium of the reactants with PRC) is much larger than the direct one k_1, and applying the steady state analysis. Calling E_{-1} the energy difference between PRC and the reactants, and E_2 the barrier between PRC and the transition state, Eq. (1) can be more explicitly written as

$$k = \kappa \frac{Q_{PRC}}{Q_T Q_{OH}} \exp\left(\frac{E_{-1}}{RT} \right) \frac{k_B T}{h} \frac{Q_{TS}}{Q_{PRC}} \exp\left(-\frac{E_2}{RT} \right) \quad (2)$$

If, as normally done, the energy of activation (ΔG) is approximated by $\Delta(E+\mathrm{ZPE})$, Eqs. (1) and (2) are identical. If the more correct expression $E_a = \Delta^{\ddagger}H^0_{298} + RT + \Delta nRT$ is used (where Δn is the change in the molecularity), a small difference arises between the two equations. Alternatively, one can use Eyring equation employing the Gibbs energy of activation $\Delta^{\ddagger}G^0_{298}$ to calculate the reaction rate (accounting correctly for the concentration, since the reaction is of second order).

$$k = \kappa \frac{k_B T}{h} \exp\left(-\frac{\Delta^{\ddagger}G^o_{298}}{RT} \right) \quad (3)$$

Table 2 presents the results we obtained using the three methodologies, Arrhenius, modified Arrhenius and Eyring. The k_{global} for each method was found taking into account the degeneracy of each process (3 for H-abstraction, 4 for o- and m- addition and 2 for p-addition, to take into account also the plane of symmetry in the ring). Percent product

Table 2 Theoretical rate constants (cm^3 mol^{-1} s^{-1}) and product fractions (%) calculated with different methods in this work, compared to experimental data and other theoretical calculations. K (global) is the total rate constant obtained from the partial ones for abstraction and addition

Reaction	Method	Basis set	Arrhenius equation				Eyring			
			E_a	K	K (global)	Product fraction (%)	$\Delta G^{\#}$	K	K (global)	Product fraction (%)
Abstraction	CBS-QB3		2.29	2.88E−15	7.68E−14	6	7.90	1.67E−14	3.48E−13	8
	G4		0.62	6.95E−14	2.26E−13	86	5.89	4.98E−13	1.57E−12	90
	M06	6-31+G(d,p)	−2.69	1.18E−12	2.35E−11	8	4.95	2.41E−12	4.12E−11	10
		6-311++G(3df,2pd)	−2.35	1.38E−12	1.03E−11	25	4.89	2.68E−12	1.80E−11	29
		cc-pVQZ	−1.46	1.76E−13	7.52E−13	54	6.12	3.39E−13	1.34E−12	61
	HATIPOGLU[a]		*1.07*	*3.11E−14*	*3.79E−13*	*9%*				
	EXPERIMENTAL		−1.99[b]	(0±0.20)E−12[b]	4.33E−13[b]					
					6.11E−12[c]					
					4.15E−12[d]					
o-Addition	CBS-QB3		−0.33	2.08E−14		58	6.96	8.13E−14		50
	G4		0.44	6.21E−15		10	7.64	2.61E−14		6
	M06	6-31+G(d,p)	−5.02	8.39E−12		77	3.93	1.37E−11		73
		6-311++G(3df,2pd)	−4.21	2.52E−12		61	4.68	3.85E−12		55
		cc-pVQZ	−3.00	9.98E−14		41	6.62	1.46E−13		35
	HATIPOGLU[a]		*0.38*	*7.61E−14*		*44%*				
m-Addition	CBS-QB3		1.10	6.50E−15		19	7.50	3.28E−14		22
	G4		2.18	1.04E−15		2	8.53	5.74E−15		2
	M06	6-31+G(d,p)	−2.81	3.70E−13		11	5.67	7.15E−13		14
		6-311++G(3df,2pd)	−2.09	1.42E−13		10	6.28	2.58E−13		12
		cc-pVQZ	−0.89	6.03E−15		3	8.17	1.06E−14		1
	HATIPOGLU[a]		*0.41*	*3.43E−14*		*20%*				
p-Addition	CBS-QB3		0.79	1.35E−14		18	7.05	7.02E−14		20
	G4		1.87	2.73E−15		2	7.94	1.57E−14		1
	M06	6-31+G(d,p)	−3.41	2.39E−12		3	4.50	5.18E−12		4
		6-311++G(3df,2pd)	−2.72	8.10E−13		3	5.16	1.71E−12		4
		cc-pVQZ	−2.08	1.30E−14		3	8.19	1.03E−14		3
	HATIPOGLU[a]		*0.01*	*9.80E−14*		*28%*				

[a]Hatipoglu et al., Ref. [16]

[b]Knispel et al., Ref. [35]

[c]Davis et al., Ref. [10]

[d]Doyle et al., Ref. [12]

fractions were obtained dividing the respective rate constant by the global one.

We included Hatipoglu's results in this table, but a word of caution is necessary. We repeated their calculations and found out that the activation energy they report, is actually the E + ZPE barrier between PRC and TS, although they use the partition function of TSs and reactants as in (1). Therefore, their results would differ from ours. Using their method, the activation energy (calculated as E + ZPE) for the H-abstraction would be − 2.66 kcal mol^{-1} close to the one we obtained at a comparably small level (M06/6-31 + G(d,p)). This level of calculations is not particularly accurate and this remains true also for the slightly larger basis set (6-311 + G(d,p)) used to improve energies. This leads, not surprisingly, to product radicals about 3–4 kcal mol^{-1} less stable than in our more accurate calculations. Notice that Hatipoglu et al. wrongly reported the H-abstraction as endothermic (see Table 2) because they did not include the water molecule generated in the reaction (see Fig. 2). Our results (− 29.0 and − 29.1 kcal mol^{-1} at the M06/cc-pVQZ and average levels, respectively) agree extremely well with the experimental enthalpy of reaction, obtained from the enthalpies of formation in the NIST Data Tables, 29.6 ± 1.3 kcal mol^{-1}. The values we obtained using the Arrhenius equation both for the activation energy (− 1.46 kcal mol^{-1}) and the global rate constant (7.52 × 10^{-13} cm^3 mol^{-1} s^{-1}) are also in good agreement with the experimental results of Knispel et al. [35], − 1.99 ± 0.26 kcal mol^{-1} and 4.33 × 10^{-13} cm^3 mol^{-1} s^{-1}.

Due to the expected errors in the barriers at the levels of theory used, the calculated rate constants may vary up to three orders of magnitude. The equation chosen to calculate the rate constant, Eqs. (1) to (3), does also affect the value, but the effect is smaller. It is important to notice that unless a very high level of theory is used, any close agreement with experiment is probably fortuitous.

The most important result in this table is that the product fraction does not depend very much on the equation chosen, but varies strongly with the level of calculation. The lower levels of theory (e.g., M06/6-31 + G(d,p), Hatipoglu's calculations) predict that the product of addition at the *ortho* position would be obtained with higher yield, followed either by the addition product in *para* or the benzyl radical. These results have been instrumental to support theoretically the experimentally observed larger yield of cresols over benzaldehyde, in the hypothesis that the latter arises from oxidation of the benzyl radical by oxygen. However, more sophisticated methods (e.g., G4 and M06/cc-pVQZ) predict that the benzyl radical would be obtained with a larger yield, ranging from 70 to 95%, depending on the method used.

Our results then seem to be consistent and in agreement with the experimental information available for the radicals, but do not explain why cresols are finally obtained in larger concentrations than benzaldehyde, since benzyl radical should be the favored intermediate radical produced. A possible explanation would be that there must exist paths leading from the benzyl radical to the cresols, in addition to the path leading from the benzyl radical to benzaldehyde. These routes were found in our calculations and are shown in Scheme 2. The full reaction mechanism explaining the discrepancy we report here, will be discussed in a forthcoming study.

4 Conclusions

We report in this paper a computational study, using several quantum mechanical methods, of the initial attack of the hydroxyl radical to the toluene molecule. Reactants, initial complexes, transition states and final products (which are actually intermediates in the much larger full reaction mechanism involving also reactions with oxygen) were determined. We calculated the enthalpies of reaction for both the H-abstraction from the CH_3 group and the OH-addition at several carbon atoms in the ring. Energies and Gibbs energies of activation at 298 K, as well as rate coefficients, were determined using Arrhenius and Eyring equations, and the results were used to calculate the fractions of intermediate benzyl and hydroxymethyl cyclohexadiene radicals.

The agreement among the results issuing from different quantum chemical methods and basis sets is generally good. Whenever experimental results were available, our theoretical results were found in good agreement with them. In particular, the reaction enthalpy computed at the M06/cc-pVQZ level (− 29.0 kcal mol^{-1}) for H-abstraction is in remarkable agreement with its experimental counterpart (− 29.6 ± 1.3 kcal mol^{-1}) and the same applies for the activation energy (− 1.46. vs. -1.99 ± 0.26 kcal mol^{-1}) and reaction rate (7.52 × 10^{-13} vs. 4.33 × 10^{-13} cm^3 mol^{-1} s^{-1}). The picture obtained strongly suggests that H-abstraction is more favorable, both thermochemically and kinetically, than OH-addition at any position in the ring. Notwithstanding this fact, the larger number of addition sites (10, when one considers all the symmetry allowed possibilities) with respect to abstraction sites (only 3) plays in favor of addition products as the most abundant ones. As Zhang et al. [22] found, abstraction should not be disregarded in a kinetic analysis of this reaction.

Our results disagree with previous less refined calculations and show that, the experimentally observed larger concentration of cresols over benzaldehyde among the final products, does not result from an initial preference of addition over abstraction. Following this idea, we were able to identify routes for the formation of cresols starting from the initial benzyl radical formed by hydrogen abstraction. The routes shown in this paper, a detailed analysis of which

is in progress, explain then the observed product fractions while, at the same time, they are in agreement with the initial preferential formation of benzyl radical over hydroxymethyl cyclohexadiene radicals.

References

1. National Academies of Sciences, Engineering, and Medicine (2016) The future of atmospheric chemistry research: remembering yesterday, understanding today, anticipating tomorrow. The National Academies Press, Washington, DC

2. Brasseur GP, Jacob DJ (2017) Modeling of atmospheric chemistry. CUP, Cambridge, UK

3. Akimoto H (2016) Atmospheric reaction chemistry. Springer, Tokyo

4. Atkinson R (1990) Gas-phase tropospheric chemistry of organic compounds: a review. Atmos Environ 24A:1–41

5. Atkinson R (1985) Kinetics and mechanisms of the gas-phase reactions of the hydroxyl radical with organic compounds under atmospheric conditions. Chem Rev 85:69–201

6. Yang Y, Shao M, Wang X, Nolscher AC, Kessel S, Guenther A, Williams J (2016) Towards a quantitative understanding of total OH reactivity: a review. Atmos Environ 134:147–161

7. Nayebzadeh M, Vahedpour M (2017) A review on reactions of polycyclic aromatic hydrocarbons with the most abundant atmospheric chemical fragments: theoretical and experimental data. Prof React Kinet Mech 42:201–220

8. Calvert JG, Atkinson R, Becker KH, Kamens RM, Seinfeld JH, Wallington TH, Yarwood G (2002) The mechanisms of atmospheric oxidation of the aromatic hydrocarbons. Oxford University Press, Oxford

9. Whitten GZ, Heo G, Kimura Y, McDonald-Buller E, Allen DT, Carter WPL, Yarwood G (2010) A new condensed toluene mechanism for carbon bond: CB05-TU. Atmos Environ 44:5346–5355

10. Davis DD, Bollinger W, Fischer S (1975) A kinetics study of the reaction of the OH free radical with aromatic compounds. 1. Absolute rate constants for reaction with benzene and toluene at 300°K. J Phys Chem 79:293–294

11. Perry RA, Atkinson R, Pitts JN Jr. (1977) Kinetics and mechanism of the gas phase reaction of hydroxyl radicals with aromatic hydrocarbons over the temperature range 296-473 K. J Phys Chem 81:296–304

12. Doyle GJ, Lloyd AC, Darnall KR, Winer AM, Pitts JN Jr. (1975) Gas phase kinetic study of relative rates of reaction of selected aromatic compounds with hydroxyl radicals in an environmental chamber. Environ Sci Tech 9:237–241

13. Hansen DA, Atkinson R, Pitts JN Jr. (1975) Rate constants for the reaction of OH radicals with a series of aromatic hydrocarbons. J Phys Chem 79:1763–1766

14. Tully FP, Ravishankara AR, Thompson RL, Nicovich JM, Shah RC, Kreutter NM, Wine PH (1981) Kinetics of the reactions of hydroxyl radical with benzene and toluene. J Phys Chem 85:2262–2269

15. Gery MW, Fox DL, Jeffries HE, Stockburger L, Weathers WS (1985) A Continuous Stirred Tank Reactor Investigation of the Gas-Phase Reaction of Hydroxyl Radicals and Toluene. Int J Chem Kinet 17:931–955

16. Hatipoglu A, Vione D, Yalcin Y, Minero C, Cinar Z (2010) Photo-oxidative degradation of toluene in aqueous media by hydroxyl radical. J Photochem Photobiol A: Chem 215:59–68

17. Zhang N, Geronimo I, Paneth P, Schindelka J, Schaefer T, Herrmann H, Richnow HH (2016) Analyzing sites of OH radical attack (ring vs. side chain) in oxidation of substituted benzenes via dual stable isotope analysis (δ13C and δ2H). Sci Tot Environ 542:484–494

18. Uc VH, García-Cruz I, Hernández-Laguna A, Vivier-Bunge A (2000) New channels in the reaction mechanism of the atmospheric oxidation of toluene. J Phys Chem A 104:7847–7855

19. Murakami Y, Oguchi T, Hashimoto K, Nosaka Y (2007) Theoretical study of the benzyl + O_2 reaction: kinetics, mechanism, and product branching ratios. J Phys Chem A 111:13200–13208

20. da Silva G, Handam MR, Bozzelli JW (2009) Oxidation of the benzyl radical: mechanism, thermochemistry, and kinetics for the reactions of benzyl hydroperoxide. J Chem Theory Comput 5:3185–3194

21. Ji Y, Zhao J, Terazono H, Misawa K, Levitt NP, Li Y, Lin Y, Peng Y, Wang Y, Duan L, Pan B, Zhang F, Feng X, An T, Marrero-Ortiz W, Secrest J, Zhang AL, Shibuya K, Molina MJ, Zhang R (2017) Reassesing the atmospheric oxidation mechanism of toluene. PNAS 114:8169–8174

22. Zhang RM, Truhlar DG, Xu X (2019) Kinetics of the toluene reaction with OH radical. Research 2019:19

23. Möller C, Plesset MS (1934) Note on an approximation treatment for many-electron systems. Phys Rev 46:618–622

24. Zhao Y, Truhlar DG (2008) The M06 suite of density functionals for main group thermochemistry, thermochemical kinetics, non-covalent interactions, excited states, and transition elements: two new functionals and systematic testing of four M06-class functionals and 12 other functionals. Theor Chem Acc 120:215–241

25. Pople JA, Nesbet RK (1954) Self-consistent orbitals for radicals. J Chem Phys 22:571–572

26. Dunning TH Jr. (1989) Gaussian basis sets for use in correlated molecular calculations. I. The atoms boron through neon and hydrogen. J Chem Phys 90:1007–1023

27. Montgomery JA Jr., Frisch MJ, Ochterski JW, Petersson GA (1999) A complete basis set model chemistry. VI. Use of density functional geometries and frequencies. J Chem Phys 110:2822–2827

28. Montgomery JA Jr., Frisch MJ, Ochterski JW, Petersson GA (2000) A complete basis set model chemistry. VII. Use of the minimum population localization method. J Chem Phys 112:6532–6542

29. Curtiss LA, Redfern PC, Raghavachari K (2007) Gaussian-4 theory. J Chem Phys 126:084108

30. Adler TB, Knizia G, Werner HW (2007) A simple and efficient CCSD(T)-F12 approximation. J Chem Phys 127:221106

31. Frisch MJ, Trucks GW, Schlegel HB, Scuseria GE, Robb MA, Cheeseman JR, Scalmani G, Barone V, Mennucci B, Petersson GA, Nakatsuji H, Caricato M, Li X, Hratchian HP, Izmaylov AF, Bloino J, Zheng G, Sonnenberg JL, Hada M, Ehara M, Toyota K, Fukuda R, Hasegawa J, Ishida M, Nakajima T, Honda Y, Kitao O, Nakai H, Vreven T, Montgomery JA Jr, Peralta JE, Ogliaro F, Bearpark M, Heyd JJ, Brothers E, Kudin KN, Staroverov VN, Keith T, Kobayashi R, Normand J, Raghavachari K, Rendell A, Burant JC, Iyengar SS, Tomasi J, Cossi M, Rega N, Millam JM, Klene M, Knox JE, Cross JB, Bakken V, Adamo C, Jaramillo J, Gomperts R, Stratmann RE, Yazyev O, Austin AJ, Cammi R,

Pomelli C, Ochterski JW, Martin RL, Morokuma K, Zakrzewski VG, Voth GA, Salvador P, Dannenberg JJ, Dapprich S, Daniels AD, Farkas O, Foresman JB, Ortiz JV, Cioslowski J, Fox DJ (2013) Gaussian 09, revision D.01. Gaussian Inc., Wallingford

32. Werner HJ, Knowles PJ, Knizia G et al (2012) Molpro, version 2012.1. University of Birmingham, Birmingham, UK

33. Uc VH, Álvarez-Idaboy JR, Galano A, García-Cruz I, Vivier-Bunge A (2006) Theoretical determination of the rate constant for OH hydrogen abstraction from toluene. J Phys Chem A 110:10155–10162

34. Ventura ON, Kieninger M, Salta Z, Kosmas AM, Barone V (2019) Enthalpies of formation of the benzyloxyl, benzylperoxyl, hydroxyphenyl radicals and related species on the potential energy surface for the reaction of toluene with the hydroxyl radical. Theor Chem Acc 138:115

35. Knispel R, Koch R, Siese M, Zetzch C (1990) Adduct formation of OH radicals with benzene, toluene, and phenol and consecutive reactions of the adducts with NO_x and O_2. Ber Bunsenges Phys Chem 94:1375–1379